Charmed-baryon production in antiproton-proton collisions within an effective Lagrangian model

R. Shyam[*]

Saha Institute of Nuclear Physics, 1/AF Bidhan Nagar, Kolkata 700064, India
(Received 23 November 2017; published 26 December 2017)

We study the productions of charmed baryons $\bar{\Lambda}_c^- \Lambda_c^+$, $\bar{\Lambda}_c^- \Sigma_c^+$, and $\bar{\Sigma}^- \Sigma_c^+$ in the antiproton-proton collisions within an effective Lagrangian model that has only the baryon-meson degrees of freedom and involves the physical hadron masses. The baryon production proceeds via the t-channel exchanges of D^0 and D^{*0} mesons in the initial collision of the antiproton with the target proton. The distortion effects in the initial and final states are accounted for by using an eikonal approximation-based procedure. We find that the reaction amplitudes of all the production channels are dominated by the D^{*0} meson-exchange diagrams. We discuss the relative roles of tensor and vector components of the D^{*0} coupling in the D^{*0} meson-exchange component of the total production cross sections. The magnitudes of the cross sections are predicted for each final state for the range of beam momenta of relevance to the $\bar{\text{P}}$ANDA experiment.

I. INTRODUCTION

The current experimental information about the production of the ground state charmed baryons has been derived mostly from the electron-positron annihilation experiments (see, e.g., Refs. [1–3]). In the near future, charmed-baryon production will be studied in the antiproton-proton ($\bar{p}p$) annihilation using the "antiproton annihilation at Darmstadt" ($\bar{\text{P}}$ANDA) experiment at the Facility for Antiproton and Ion Research (FAIR) in GSI, Darmstadt (see, e.g., Ref. [4]). The advantage of using antiprotons in the study of charmed baryons is that in $\bar{p}p$ collisions the production of extra particles is not needed for the charm conservation, which reduces the threshold energy as compared to, say, pp collisions. The beam momenta of antiprotons in this experiment will be well above the thresholds of the productions of $\bar{\Lambda}_c^- \Lambda_c^+$ and $\bar{\Sigma}^- \Sigma_c^+$ charmed baryons in the $\bar{p}p$ collisions. For the planning of this experiment, reliable theoretical estimates of the cross sections of these reactions would be of crucial importance. The production rates of these reactions are also the key requirement in the implementation of other programs [5] of the $\bar{\text{P}}$ANDA experiment, e.g., spectroscopy of charmed hadrons (see, e.g., Ref. [4]), production of charm hypernuclei [6,7], D mesonic nuclei [8–11], and medium effects on the charmed-hadron properties [12–17].

The investigations of the production of heavy flavor hadrons provide an additional handle for the understanding of quantum chromodynamics, the fundamental theory of the strong interaction. The presence of the heavy charm quark along with the light quark(s) leads to two energy scales in such systems. This allows the construction of an effective theory where one can actually calculate a big portion of the relevant physics using the perturbation theory and renormalization-group techniques [18–20].

Calculations of the cross sections of the $\bar{\Lambda}_c^- \Lambda_c^+$ production in the $\bar{p}p$ collisions have been reported in several publications using a variety of models [21–28]. They employ varying degrees of freedom ranging from quarks [21–24,27] to meson baryon [25,26,28] in the description of this reaction. However, the magnitudes of the predicted cross sections are strongly model dependent. On the other hand, calculations for other charmed-baryon channels have been reported only by a few authors. In Ref. [27], total cross sections have been given for $\bar{\Sigma}_c^- \Lambda_c^+$ and $\bar{\Sigma}_c^- \Sigma_c^+$ channels, which are obtained by integrating the differential cross sections $d\sigma/dt$ (t is the momentum transfer) over a limited range of t. In ref. [23], $d\sigma/dt$ are provided for these final states, but the integrated cross sections are not given.

In Ref. [29], cross sections have been presented for the charm-production channels $\bar{p}p \to \bar{\Lambda}_c^- \Sigma_c^+$, $\bar{\Sigma}_c^- \Sigma_c^+$, $\bar{\Sigma}_c^0 \Sigma_c^0$, $\bar{\Sigma}_c^{--} \Sigma_c^{++}$, $\bar{\Xi}_c^- \Xi_c^+$, and $\bar{\Xi}_c^0 \Xi_c^0$ within the Jülich meson-exchange model that was employed earlier [30,31] to investigate the $\bar{p}p \to \bar{\Lambda}\Lambda$ reaction. In this model, a coupled-channels framework is used that allows to take into account the initial- and final-state interactions in a rigorous way. The reaction proceeds via exchanges of appropriate mesons between $\bar{p}$ and p leading to the final antibaryon-baryon states. For calculating the cross sections for the $\bar{\Sigma}_c^0 \Sigma_c^0$, $\bar{\Sigma}_c^{--} \Sigma_c^{++}$, $\bar{\Xi}_c^- \Xi_c^+$, and $\bar{\Xi}_c^0 \Xi_c^0$ final states, two-step mechanisms have been invoked in Ref. [29]. However, in this reference, cross sections are reported only for beam momenta very close to the respective threshold of each final state.

In Ref. [28], the $\bar{p}p \to \bar{\Lambda}_c^- \Lambda_c^+$ reaction has been studied within a single-channel effective Lagrangian model (see, e.g., Refs. [32,33]), where this reaction is described as a sum of the t-channel D^0 and D^{*0} meson-exchange

*radhey.shyam@saha.ac.in

diagrams. The s- and u-channel resonance excitation terms are suppressed, as no resonance is known with energy in excess of 3.0 GeV having branching ratios for decays to the charmed-baryon channels. Furthermore, the direct $\bar{p}p$ annihilation into charmed-baryon final states via the contact diagrams is also suppressed due to the Okubo-Zweig-Iizuka condition.

The aim of this paper is to extend the model of Ref. [28] to calculate the cross sections of the $\bar{p}p \to \bar{\Lambda}_c^- \Sigma_c^+$ and $\bar{p}p \to \bar{\Sigma}_c^- \Sigma_c^+$ reactions. We provide predictions for the cross sections for beam momenta ($\bar{p}_{\text{lab}}$) ranging from threshold to 18 GeV/c in each case. Therefore, the range of $\bar{p}_{\text{lab}}$ of interest to the $\overline{\text{P}}$ANDA experiment is well covered. As in Ref. [28], these reactions are described as a sum of t-channel D^0 and D^{*0} meson-exchange diagrams. The s- and u-channel resonance excitation diagrams are suppressed due to the same reason as stated in the previous paragraph. Of course, like the $\bar{\Lambda}_c^- \Lambda_c^+$ channel, experimental data also do not exist at present for the other charmed-baryon channels.

The amplitudes calculated in the effective Lagrangian model include basically only the Born terms. However, from the studies of the $\bar{p}p \to \bar{\Lambda}_c^- \Lambda_c^+$ reaction, it is known that there is a strong sensitivity of the cross sections to the distortion effects in the initial and final states [30,31,34–42]. We account for such effects approximately by using an eikonal approximation-based procedure.

In the next section, we present our formalism. The results and discussions of our work are given in Sec. III. Finally, the summary and conclusions of this study are presented in Sec. IV.

II. FORMALISM

To evaluate various amplitudes for the processes shown in Fig. 1, we have used the effective Lagrangians at the charmed-baryon-meson-nucleon vertices, which are taken from Refs. [43–45]. For the pseudoscalar D meson exchange vertices, we have

$$\mathcal{L}_{BDN} = ig_{BDN}\bar{\psi}_B i\gamma_5 \psi_N \phi_D + \text{H.c.}, \qquad (1)$$
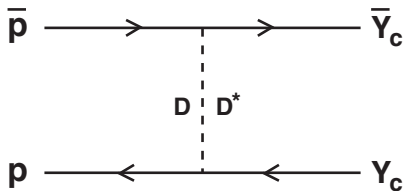

FIG. 1. Graphical representation of the model used to describe the $\bar{p} + p \to \bar{Y}_c + Y_c$ reaction, where Y_c represents a charmed baryon. D and D^*, in the intermediate line, represent the exchanges of D pseudoscalar and D^* vector mesons, respectively. In cases of $\bar{\Lambda}_c^- \Lambda_c^+$, $\bar{\Lambda}_c^- \Sigma_c^+$, and $\bar{\Sigma}_c^- \Sigma_c^+$, final states D and D^* correspond to D^0 and D^{*0} mesons, respectively.

where ψ_B and ψ_N are the charmed-baryon and nucleon (antinucleon) fields, respectively. In Eq. (1), ϕ_D is the D meson field and g_{BDN} represents the vertex coupling constant.

For the vector meson D^* exchange vertices, the effective Lagrangian is

$$\mathcal{L}_{BD^*N} = g_{BD^*N}\bar{\psi}_B \gamma_\mu \psi_N \theta_{D_*}^\mu + \frac{f_{BD^*N}}{4M}\bar{\psi}_B \sigma_{\mu\nu} \psi_N F_{D^*}^{\mu\nu} + \text{H.c.}, \qquad (2)$$

where $\theta_{D_*}^\mu$ is the vector meson field, with field strength tensor $F_{D^*}^{\mu\nu} = \partial^\mu \theta_{D^*}^\nu - \partial^\nu \theta_{D^*}^\mu$. In Eq. (2), $\sigma_{\mu\nu}$ is the usual tensor operator. The vector and tensor couplings are defined by g and f, respectively. Their values at various vertices were adopted from Refs. [43,44] as shown in Table I. The same couplings were used for the vertices involving both the proton and the antiproton. It was shown in Ref. [28] that the exchange of D^{*0} dominates the $\Lambda_c^+ \bar{\Lambda}_c^-$ production reaction in the $\bar{p} - p$ collisions even for beam momenta closer to the production threshold.

The coupling constants adopted by us at various vertices involved in the t-channel diagrams were determined in Refs. [44,46,47], by using the SU(4) symmetry arguments in the description of the exclusive charmed-hadron production in the $\bar{D}N$ and DN scattering within a one-boson-exchange picture. While we acknowledge that the SU(4) symmetry will not hold rigorously, the deviations from the SU(4) coupling constants in the charm sector have been reported to be highly model dependent [48]. Recent calculations within light-cone sum rules suggest that deviations from the SU(4) values of the relevant coupling constants are not more than factors of 2 [27]. On the other hand, in the constituent quark model calculations using the $^3P_0$ quark-pair creation mechanism, the deviations are at the most of the order of 30% [49].

The off-shell behavior of the vertices is regulated by introducing form factors. Without them, calculations with Born terms strongly overestimate the cross section at higher energies. Therefore, such contributions will have to be quenched with form factors. Another motivation for introducing form factors is that at higher energies one may expect sensitivity to the underlying quark structure of the

TABLE I. Coupling constants at the BD^0N and $BD^{*0}N$ vertices. These are taken from Refs. [43,44].

Vertex	Exchanged meson mass (MeV)	Exchanged meson width (MeV)	$g_{DBN}/\sqrt{4\pi}$	$f_{DBN}/\sqrt{4\pi}$
$ND^0\Lambda_c^+$	1864.84	…	3.943	…
$ND^{*0}\Lambda_c^+$	2006.96	2.1	1.590	5.183
$ND^0\Sigma_c^+$	1864.84	…	0.759	…
$ND^{*0}\Sigma_c^+$	2006.96	2.1	0.918	−2.222

hadrons. Because this physics is not included explicitly in our model, we can only account for it by introducing the phenomenological form factors at the vertices. In our approach, the form factors are not known *a priori* and thus they introduce a certain arbitrariness in the calculations. In the current paper, we limit ourselves to dipole form factors (see, e.g., Refs. [32,33]) at the vertices involving the pseudoscalar D meson exchange because of their simplicity

$$F_i(q_i) = \frac{\lambda_i^2 - m_{D_i}^2}{\lambda_i^2 - q_{D_i}^2}, \tag{3}$$

where q_{D_i} is the momentum of the ith exchanged meson with mass m_{D_i}. λ_i is the corresponding cutoff parameter, which governs the range of suppression of the contributions of high momenta carried out via the form factor. We chose a value of 3.0 GeV for λ_i at both the vertices. The same λ_i was also used in the monopole form factor employed in the studies presented in Refs. [25,26,43].

However, at the vertices involving the exchange of the vector meson D^*, we have used a different functional form of the form factor

$$F_i(q_i) = \left[\frac{\lambda_i^4}{\lambda_i^4 + (q_i^2 - m_i^2)^2} \right]. \tag{4}$$

The argumentation for this different choice is presented in the discussion of the Σ-photoproduction results in Ref. [50]. Often, different functional forms and cutoff values are introduced for t-channel form factors [51–53]. Although this can easily be motivated, it introduces additional model dependence and increases the number of free parameters. To limit the overall number of parameters, we have taken the form factor given by Eq. (3), with a cutoff parameter λ_i of 3.0 GeV for all the graphs involving the D meson exchange, and that given by Eq. (4), with a λ_i of 2.7 GeV for all the terms involving the D^* meson exchange. Because the experimental data are not yet available for the reactions under investigation in this paper, it is not possible to put a more definite constraint on these quantities. Therefore, we restrict ourselves to these choices of the form factors and the λ_i values.

For calculating the amplitudes, we require the propagators for the exchanged mesons. For the D and D^* mesons, the propagators are given by

$$G_D(q) = \frac{i}{q^2 - m_D^2}, \tag{5}$$

$$G_{D^*}^{\mu\nu}(q) = -i\left(\frac{g^{\mu\nu} - q^\mu q^\nu / q^2}{q^2 - (m_{D^*} - i\Gamma_{D^*}/2)^2} \right). \tag{6}$$

In Eq. (6), Γ_{D^*} is the total width of the D^* meson, which is given in Table I, taken from the latest Particle Data Group estimates [54].

After having established the effective Lagrangians, coupling constants, and forms of the propagators, the amplitudes of various diagrams can be written by following the well-known Feynman rules. The signs of these amplitudes are fixed by those of the effective Lagrangians, the coupling constants, and the propagators as described above. These signs are not allowed to change anywhere in the calculations.

Next, we describe how the initial- and final-state interactions are taken into account in our calculations. We note that, for the $\bar{p}p$ initial state, the annihilation channel is almost as strong as the elastic scattering channel. This large depletion of the flux can be accounted for by introducing absorptive potentials that are used in optical model or in coupled-channels approaches [25,30,31,38,42]. In this work, we do not employ such a detailed treatment. Instead, we use a procedure that was originated by Sopkovich [55]. In this method, the transition amplitude with distortion effects is written as

$$T^{\bar{p}p \to \bar{Y}_c Y_c} = \sqrt{\Omega^{\bar{p}p}} T_{\text{Born}}^{\bar{p}p \to \bar{Y}_c Y_c} \sqrt{\Omega^{\bar{Y}_c Y_c}} \tag{7}$$

where $T_{\text{Born}}^{\bar{p}p \to \bar{Y}_c Y_c}$ is the transition matrix calculated within the Born approximation, and $\Omega^{\bar{p}p}$ and the $\Omega^{\bar{Y}_c Y_c}$ are the matrices describing the initial- and final-state elastic scatterings, respectively. Their effects are to dampen the wave functions and hence the amplitudes. For the case of the $\bar{p}p \to \bar{\Lambda}_c^- \Lambda_c^+$ reaction, it was shown in Ref. [25] that, because of the strong absorption in the initial channel, the results turned out to be rather insensitive to the final-state $\bar{\Lambda}_c^- \Lambda_c^+$ interactions. In fact, even if the final-state interactions (FSIs) were ignored totally, the total cross sections did not change by more than 10%–15%. We assume this to be true also for the other charmed-baryon final states as well. Therefore, in order to keep the number of free parameters small, we decided to fully neglect FSIs and concentrate only on the initial-state interaction in our calculations of the cross sections of all the charmed-baryon-antibaryon final channels.

For the present purpose, we neglect the real part of the proton-antiproton interaction and describe the strong absorption by an imaginary potential of Gaussian shape with range parameter μ and strength V_0

$$U(b, z) = V_0 \exp(-\mu^2 r^2), \tag{8}$$

where μ is the range parameter and V_0 the strength of the potential. In Eq. (8), $r^2 = b^2 + z^2$, with b being the impact parameter of the collision. By using the eikonal approximation, the corresponding attenuation integral can be evaluated in a closed form. Similar to Refs. [40,55], we obtain for $\Omega^{\bar{p}p}$

$$\Omega^{\bar{p}p} = \exp\left[\frac{-\sqrt{\pi}EV_0}{\mu K} \exp(-\mu^2 b^2) \right], \tag{9}$$

where E and k are the center of mass energy and momentum of the particular channel, respectively. In our numerical calculations, we have used $V_0 = 0.8965\,\text{GeV}$ and $\mu = 0.3369\,\text{GeV}$. For the impact parameter, we have taken a value $0.327\,\text{GeV}^{-1}$. These parameters are the same as those used in Refs. [28,53]. As shown in Ref. [28], with these parameters, it was possible to get cross sections for the $\bar{\Lambda}_c^- \Lambda_c^+$ production in close agreement with those calculated within the coupled-channels approach of Ref. [25], where distortion effects are rigorously treated.

Although the parameters V_0 and μ may change with energy, we have made them global; that is, they remain the same at all the energies corresponding to all the final channels. Thus, we have only three fixed parameters in our calculations of the initial-state distortion effects.

III. RESULTS AND DISCUSSIONS

In Fig. 2, we investigate the role of various meson-exchange processes in the total cross sections (σ_tot) of the reactions $\bar{p}p \to \bar{\Lambda}_c^- \Lambda_c^+$ [Fig. 2(a)] and $\bar{p}p \to \bar{\Lambda}_c^- \Sigma_c^+$ [Fig. 2(b)] as a function of $\bar{p}$ beam momenta. Although the predictions for the cross sections of the $\bar{p}p \to \bar{\Lambda}_c^- \Lambda_c^+$ reaction were presented already in Ref. [28], we give it here again for the purpose of comparison with the σ_tot of
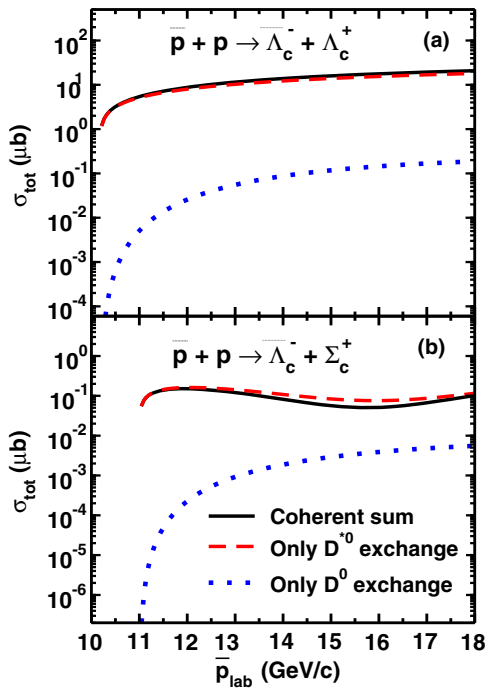

FIG. 2. Total cross section for $\bar{p}p \to \bar{\Lambda}_c^- \Lambda_c^+$ (a) and $\bar{p}p \to \bar{\Lambda}_c^- \Sigma_c^+$ (b) reactions as a function of the beam momentum. It is to be noted that cross sections for the reaction $\bar{p}p \to \bar{\Sigma}_c^- \Lambda_c^+$ are the same as those shown in Fig. 2(b). In these figures, the contributions of D^0 and D^{*0} exchange processes are shown by dotted and dashed lines, respectively. The solid line represents their coherent sum.

other charmed-baryon channels. Also, because in this paper we have used a different form factor at the vertices involving D^{*0} meson exchange, it would be of interest to have results also for this charmed-baryon final state. In Figs. 2(a) and 2(b), total cross sections σ_tot are shown for $\bar{p}_\text{lab}$ varying in the range of threshold to $18\,\text{GeV}/c$ that covers the beam momenta of interest to the $\bar{\text{P}}$ANDA experiment. We note that, for both the reactions, the cross sections increase gradually as $\bar{p}_\text{lab}$ goes above the thresholds of the respective reactions. The threshold beam momenta for $\bar{p}p \to \bar{\Lambda}_c^- \Lambda_c^+$ and $\bar{p}p \to \bar{\Lambda}_c^- \Sigma_c^+$ reactions are 10.162 and $10.99\,\text{GeV}/c$, respectively. For $\bar{p}_\text{lab}$ around $15\,\text{GeV}/c$, which is the beam momentum region of interest to the $\bar{\text{P}}$ANDA experiment, σ_tot for the $\bar{p}p \to \bar{\Lambda}_c^- \Lambda_c^+$ reaction is about one order of magnitude larger than that for the $\bar{p}p \to \bar{\Lambda}_c^- \Sigma_c^+$ reaction. The likely reasons for this difference are the smaller coupling constants at the $ND^*\Sigma_c^+$ vertices and the negative interference between the D^{*0} and D^0 exchange terms in case of the $\bar{\Lambda}_c^- \Sigma_c^+$ final state.

In Figs. 2(a) and 2(b), we note that the D^{*0} exchange process dominates the cross sections for both the final states. The D^0 exchange contributions are nearly 2 orders of magnitude smaller than those of the D^{*0} exchange in case of the $\bar{\Lambda}_c^- \Lambda_c^+$ final state and nearly an order of magnitude for the $\bar{\Lambda}_c^- \Sigma_c^+$ final state in the region of higher beam momenta. Interestingly, we notice in Fig. 2(b) that, even though for $\bar{p}_\text{lab}$ beyond $14\,\text{GeV}/c$ the individual contributions of the D^0 exchange terms are at least 1 order of magnitude smaller, they still influence the total cross sections significantly through the interference terms that are destructive in this case.

The domination of the D^{*0} meson-exchange terms is related to the presence of the strong tensor part in the $ND^{0*}Y_c^+$ couplings. We note from Table I that the ratio of tensor to vector coupling constants of these vertices is in the vicinity of three. Also there is additional momentum dependence induced by the derivative coupling in the tensor interaction part of the effective Lagrangian. In Figs. 3(a) and (3b), we show the individual contributions of tensor and vector terms to the D^{*0} meson-exchange component of the total cross section ($\sigma_\text{tot}^{D^{*0}}$) for the reactions $\bar{p}p \to \bar{\Lambda}_c^- \Lambda_c^+$ and $\bar{p}p \to \bar{\Lambda}_c^- \Sigma_c^+$, respectively. It is clear that the tensor coupling terms make the dominant contributions to $\sigma_\text{tot}^{D^{*0}}$ for both the reactions. Although the vector coupling terms are relatively quite small in themselves, they can influence the cross sections $\sigma_\text{tot}^{D^{*0}}$ significantly through the interference terms. For the $\bar{p}p \to \bar{\Lambda}_c^- \Lambda_c^+$ reaction, the interference of tensor and vector terms is constructive that enhances $\sigma_\text{tot}^{D^{*0}}$, particularly at higher beam momenta. However for the $\bar{p}p \to \bar{\Lambda}_c^- \Sigma_c^+$ reaction, this interference is destructive that reduces $\sigma_\text{tot}^{D^{*0}}$ rather sharply in this region.

It would be of interest to compare our cross sections for these two channels to those published previously. In
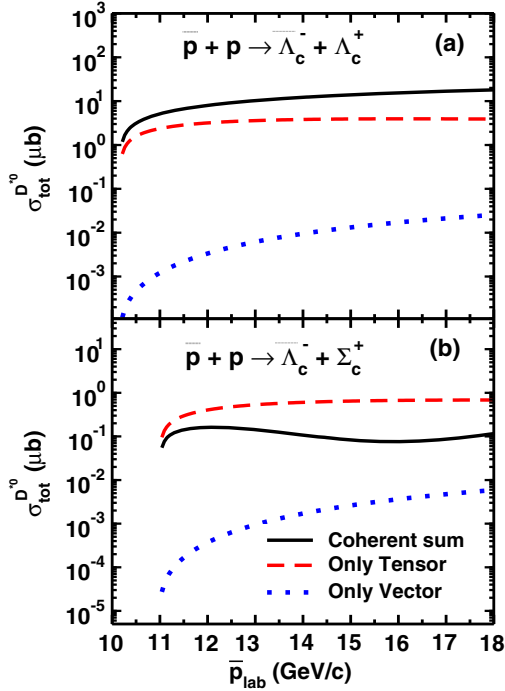
FIG. 3. Contributions of the vector and tensor coupling terms to the D^{*0} meson-exchange component of the total cross section ($\sigma_{\text{tot}}^{D^{*0}}$) for reactions $\bar{p}p \to \bar{\Lambda}_c^- \Lambda_c^+$ (a) and $\bar{p}p \to \bar{\Lambda}_c^- \Sigma_c^+$ (b) as a function of the antiproton beam momentum. The contributions of the tensor and vector terms are shown by the dashed and dotted lines, respectively. The solid line represents their coherent sum.

Ref. [29], the cross section σ_{tot} are given for the $\bar{\Lambda}_c^- \Lambda_c^+$ channel for $\bar{p}_{\text{lab}}$ in the range of threshold to 11.5 GeV/c. In this range of beam momenta, our σ_{tot} for this reaction are approximately in agreement with those calculated within the meson-exchange model (MEM) in Ref. [29]. On the other hand, for the $\bar{\Lambda}_c^- \Sigma_c^+$ channel, our cross sections are smaller than the MEM cross sections of Ref. [29] by factors of about 10. In Ref. [27], σ_{tot} for the $\bar{\Lambda}_c^- \Lambda_c^+$ and $\bar{\Lambda}_c^- \Sigma_c^+$ channels are given around the $\bar{p}_{\text{lab}}$ of 15 GeV. These authors have performed their calculations within a nonperturbative quark-gluon string model [22] employing the baryon-meson coupling constants from light-cone sum rules. Our cross sections are at least an order of magnitude larger than those of Ref. [27] for both the channels. Similarly, the cross sections for the $\bar{\Lambda}_c^- \Lambda_c^+$ production channel reported in Refs. [22–24] are also significantly smaller than those predicted in our study. Thus, differences between our cross sections and those of Refs. [22–24,27] are substantial for beam momenta relevant to the $\bar{P}$ANDA experiment.

In Fig. 4, we investigate the relative contributions of D^0 and D^{*0} meson-exchange processes to the total cross section σ_{tot} of the $\bar{p}p \to \bar{\Sigma}_c^- \Sigma_c^+$ reaction. We first notice that the magnitudes of the σ_{tot} are further reduced in this case as compared to those of the $\bar{\Lambda}_c^- \Sigma_c^+$ production. This is due to the fact that now there are two $ND^*\Sigma_c^+$ vertices
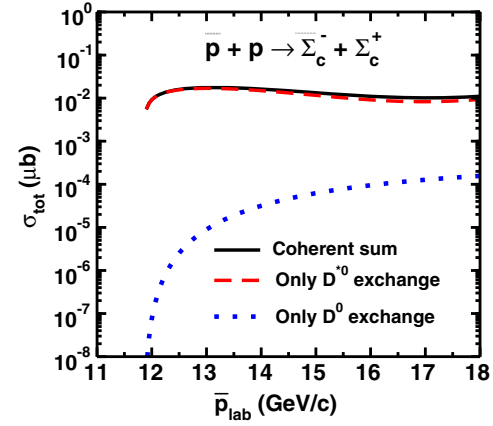

FIG. 4. Contributions of the D^0 (dotted line) and D^{*0} (dashed line) meson exchange processes to the total cross section of the $\bar{p}p \to \bar{\Sigma}_c^- \Sigma_c^+$ reaction (solid line) as a function of the antiproton beam momentum.

having coupling constants smaller than that of the $ND^{0*}\Lambda_c^+$ vertex. Like the results presented in Fig. 2, in this case also the D^{*0} exchange terms make the predominant contributions to σ_{tot}. At the beam momenta around 15 GeV/c, the D^0 meson-exchange terms are about 2 order magnitudes smaller than those of the D^{0*} exchange. At beam momenta closer to the threshold ($\bar{p}_{\text{lab}} = 11.85$ GeV/c), the differences between the contributions of two meson-exchange terms are even bigger.

In Fig. 5, the relative contributions of the vector and tensor terms of the $ND^{0*}\Sigma_c^+$ couplings to cross section $\sigma_{\text{tot}}^{D^{*0}}$ are shown. We see that the tensor component of the coupling dominates $\sigma_{\text{tot}}^{D^{*0}}$. It is further noted that, like the results shown in Fig. 3(b), the interference between tensor and vector
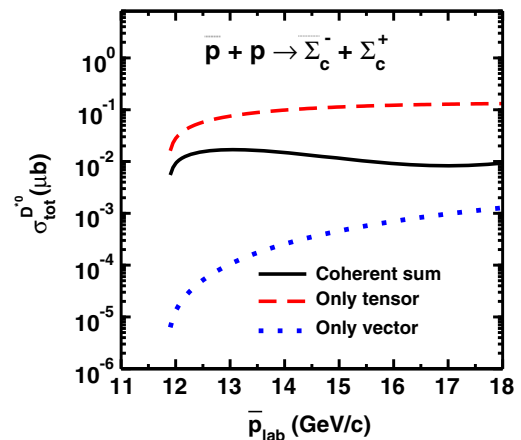

FIG. 5. Contributions of the vector and tensor coupling terms to the D^{*0} exchange component of the cross sections ($\sigma_{\text{tot}}^{D^{*0}}$) for the $\bar{p}p \to \bar{\Sigma}_c^- \Sigma_c^+$ reaction as a function of the beam momentum $\bar{p}_{\text{lab}}$. The tensor and vector terms are shown by the dashed and dotted lines, respectively. The solid line represents their coherent sum.

amplitudes is destructive. This effect significantly reduces the magnitude of $\sigma_{\mathrm{tot}}^{D^{*0}}$ at higher beam momenta.

It may be possible to calculate the cross sections of the $\bar{p}p \to \bar{\Sigma}_c^0 \Sigma_c^0$ and $\bar{p}p \to \bar{\Sigma}_c^{--} \Sigma_c^{++}$ channels also by invoking some two-step mechanism as is done in Ref. [29]. However, it may not be feasible in the version of the effective Lagrangian model presented in this paper. Nevertheless, the magnitudes of the cross sections for these channels are similar to those of the $\bar{\Sigma}_c^- \Sigma_c^+$ channel as is shown in Ref. [29].

IV. SUMMARY AND CONCLUSIONS

In summary, we studied the $\bar{p}p \to \bar{\Lambda}_c^- \Lambda_c^+$, $\bar{p}p \to \bar{\Lambda}_c^- \Sigma_c^+$, $\bar{p}p \to \bar{\Sigma}_c^- \Lambda_c^+$, and $\bar{p}p \to \bar{\Sigma}_c^- \Sigma_c^+$ reactions using a phenomenological effective Lagrangian model that involves the meson-baryon degrees of freedom. The charmed-baryon production mechanism is described by the t-channel D^0 and D^{*0} meson-exchange diagrams, while largely phenomenological initial- and final-state interactions were used to account for the distortion effects. The coupling constants at various vertices have been taken from the DN and $\bar{D}N$ scattering studies reported in Refs. [44,46,47]. The off-shell corrections at the D^0 meson vertices are incorporated by introducing monopole form factors, which was taken to be the same for all the cases. However, at the vertices involving the D^{*0} meson exchange, a type of quadrupole form factor has been used. The shapes of the form factors and the values of the cutoff parameters appearing therein have been held fixed for all the final charmed-baryon production channels.

In the range of beam momenta of interest to the $\bar{\mathrm{P}}$ANDA experiment, the total cross sections are largest for the $\bar{\Lambda}_c^- \Lambda_c^+$ production channel. For beam momenta not too far from the threshold, the cross sections for this final state as predicted by our model are similar to those obtained within the Jülich meson-exchange model as reported in Ref. [29]. The production cross sections for the $\bar{\Lambda}_c^- \Sigma_c^+$ and $\bar{\Sigma}_c^- \Sigma_c^+$ final states are smaller than those of the $\bar{\Lambda}_c^- \Lambda_c^+$ channel by factors of the order of 10 and 100, respectively. The reasons for this is traced back to the large negative interference between the vector and tensor parts of the D^{*0} meson-exchange term and relatively smaller coupling constants of the $ND^{*0}\Sigma_c^+$ vertices. Furthermore, even though our cross sections for these channels are smaller than those calculated within the meson-exchange model of Ref. [29], they are still larger than those of Refs. [22–24,27]. Because these earlier calculations have used different types of approaches, which employ quark-model-based ingredients in their calculations, it is not trivial to locate the reason for the large

difference seen between their and our results. The $\bar{\mathrm{P}}$ANDA experiment for these reactions should provide an opportunity to understand this difference once the FAIR facility is operational. If the cross sections are as large as predicted in our calculations, as well as in those of the meson-exchange model of Ref. [29], the experimental requirements may perhaps become less stringent for their measurements at $\bar{\mathrm{P}}$ANDA.

We found that the vector meson (D^{*0}) exchange terms dominate the cross sections for all the reaction channels in the entire range of beam momenta. The reasons for the large strength of this exchange process are the strong tensor coupling of the vector mesons (similar to the large tensor coupling of the ρ meson in NN interactions) and the additional momentum dependence introduced by the derivative part of the corresponding interaction. Although the individual contributions of the D^0 exchange terms are relatively weak, they can still affect the total cross sections through the interference terms.

We treated the initial- and final-state interactions within an eikonal approximation-based phenomenological method. Generally, the parameters of this model are constrained by fitting to the experimental data. Because of the lack of any experimental information, it has not been possible to test our model thoroughly. Therefore, there may be some uncertainty in the absolute magnitudes of our cross sections. Nevertheless, our near-threshold cross sections for the $\bar{\Lambda}_c^- \Lambda_c^+$ production channel are very close to those of Refs. [29], where distortion effects have been treated more rigorously within a coupled-channels approach. There may also be some uncertainty in our cross sections coming from the shapes of the form factors and the values of the cutoff parameter involved therein. In models like ours, choice for these quantities is guided by their ability to reproduce the experimental data [56], which is not feasible at this stage for the charmed-baryon production. We have tried to minimize the effects of such uncertainties to some extent by using the same shape of the form factor and the same value of the cutoff parameter in calculations of all the final charmed-baryon channels. Hopefully, concrete experiments that are likely to be pursued with the $\bar{\mathrm{P}}$ANDA experiment at FAIR will help in removing most of these uncertainties.

[1] M. S. Dubrovin (CLEO Collaboration), arXiv:hep-ex/0305006.
[2] V. Ziegler (*BABAR* Collaboration), AIP Conf. Proc. **1374**, 577 (2011), and references therein.
[3] Y. Kato (Belle Collaboration), *Proc. Sci.*, Hadron2013 (2014), 053, and references therein.
[4] U. Wiedner, Prog. Part. Nucl. Phys. **66**, 477 (2011).
[5] W. Erni *et al.*, arXiv:0903.3905.
[6] C. B. Dover and S. H. Kahana, Phys. Rev. Lett. **39**, 1506 (1977).
[7] R. Shyam and K. Tsushima, Phys. Lett. B **770**, 236 (2017).
[8] K. Tsushima, D. H. Lu, A. W. Thomas, K. Saito, and R. H. Landau, Phys. Rev. C **59**, 2824 (1999).
[9] C. Garcia-Recio, J. Nieves, and L. Tolos, Phys. Lett. B **690**, 369 (2010).
[10] C. Garcia-Recio, J. Nieves, L. L. Salcedo, and L. Tolos, Phys. Rev. C **85**, 025203 (2012).
[11] J. Yamagata-sekihara, C. Garcia-Recio, J. Nieves, L. L. Salcedo, and L. Tolos, Phys. Lett. B **754**, 26 (2016).
[12] K. Tsushima and F. C. Khanna, Phys. Lett. B **552**, 138 (2003).
[13] K. Tsushima and F. C. Khanna, J. Phys. G **30**, 1765 (2004).
[14] C. E. Jimenez-Tejero, L. Tolos, I. Vidaña, and A. Ramos, Few-Body Syst. **50**, 351 (2011).
[15] L. Tolos, Int. J. Mod. Phys. E, **22**, 1330027 (2013).
[16] G. Krein, AIP Conf. Proc. **1701**, 020012 (2016).
[17] R. Shyam and K. Tsushima, Phys. Rev. D **94**, 074041 (2016).
[18] R. Sommer, Nucl. Part. Phys. Proc. **261–262**, 338 (2015).
[19] A. V. Manohar and M. B. Wise, *Cambridge Monographs on Particle Physics, Nuclear Physics and Cosmology* (Cambridge University Press, Cambridge, England, 2000), Vol. 10.
[20] M. Neubert, Phys. Rep. **245**, 259 (1994).
[21] P. Kroll, B. Quadder, and W. Schweiger, Nucl. Phys. **B316**, 373 (1989).
[22] A. B. Kaidalov and P. E. Volkovitsky, Z. Phys. C **63**, 517 (1994).
[23] A. I. Titov and B. Kämpfer, Phys. Rev. C **78**, 025201 (2008).
[24] A. T. Goritschnig, P. Kroll, and W. Schweiger, Eur. Phys. J. A **42**, 43 (2009).
[25] J. Haidenbauer and G. Krein, Phys. Lett. B **687**, 314 (2010).
[26] J. Haidenbauer and G. Krein, Few-Body Syst. **50**, 183 (2011).
[27] A. Khodjamirian, Ch. Krein, Th. Mannel, and Y.-M. Wang, Eur. Phys. J. A **48**, 31 (2012).

[28] R. Shyam and H. Lenske, Phys. Rev. D **90**, 014017 (2014).
[29] J. Haidenbauer and G. Krein, Phys. Rev. D **95**, 014017 (2017).
[30] J. Haidenbauer, T. Hippchen, K. Holinde, B. Holzenkamp, V. Mull, and J. Speth, Phys. Rev. C **45**, 931 (1992).
[31] J. Haidenbauer, K. Holinde, V. Mull, and J. Speth, Phys. Rev. C **46**, 2158 (1992).
[32] R. Shyam, Phys. Rev. C **60**, 055213 (1999).
[33] R. Shyam and U. Mosel, Phys. Rev. C **67**, 065202 (2003).
[34] H. Genz and S. Tatur, Phys. Rev. D **30**, 63 (1984).
[35] F. Tabakin and R. A. Eisenstein, Phys. Rev. C **31**, 1857 (1985).
[36] P. Kroll and W. Schweiger, Nucl. Phys. **A474**, 608 (1987).
[37] M. Burkardt and M. Dillig, Phys. Rev. C **37**, 1362 (1988).
[38] M. Kohono and W. Weise, Nucl. Phys. **A454**, 429 (1986).
[39] G. Brix, H. Genz, and S. Tatur, Phys. Rev. D **39**, 2054 (1989).
[40] W. Roberts, Z. Phys. C **49**, 633 (1991).
[41] F. Tabakin, R. A. Eisenstein, and Y. Lu, Phys. Rev. C **44**, 1749 (1991).
[42] M. A. Alberg, E. M. Henley, L. Wilets, and P. D. Kunz, Nucl. Phys. **A560**, 365 (1993).
[43] T. J. Hobbs, J. T. Londergan, and W. Melnitchouk, Phys. Rev. D **89**, 074008 (2014).
[44] J. Haidenbauer, G. Krein, U.-G. Meissner, and L. Tolos, Eur. Phys. J. A **47**, 18 (2011).
[45] A. Müller-Groeling, K. Holinde, and J. Speth, Nucl. Phys. **A513**, 557 (1990).
[46] J. Haidenbauer, G. Krein, U.-G. Meissner, and A. Sibirtsev, Eur. Phys. J. A **33**, 107 (2007).
[47] J. Haidenbauer, G. Krein, U.-G. Meissner, and A. Sibirtsev, Eur. Phys. J. A **37**, 55 (2008).
[48] G. Krein, *Proc. Sci.*, Confinement X (2012) 144.
[49] G. Krein, Eur. Phys. J. Web Conf. **73**, 05001 (2014).
[50] A. Usov and O. Scholten, Phys. Rev. C **72**, 025205 (2005).
[51] R. Shyam and O. Scholten, Phys. Rev. C **78**, 065201 (2008).
[52] J. Haidenbauer and G. Krein, Phys. Rev. D **89**, 114003 (2014).
[53] R. Shyam and H. Lenske, Phys. Rev. D **93**, 034016 (2016).
[54] C. Patrignani *et al.* (Particle Data Group), Chin. Phys. C **40**, 100001 (2016), and 2017 update.
[55] N. J. Sopkovich, Nuovo Cimento **26**, 186 (1962).
[56] R. Shyam, O. Scholten, and H. Lenske, Phys. Rev. C **81**, 015204 (2010).